small methods
www.small-methods.com

Designing Low Tortuosity Electrodes through Pattern Optimization for Fast-Charging

*Ying Wang, Yuxuan Zhang, Daxian Cao, Tongtai Ji, Haoze Ren, Guanyi Wang, Qingliu Wu, and Hongli Zhu**

The development of fast-charging technologies is crucial for expediting the progress and promotion of electric vehicles. In addition to innovative material exploration, reduction in the tortuosity of electrodes is a favored strategy to enhance the fast-charging capability of lithium-ion batteries by optimizing the ion-transfer kinetics. To realize the industrialization of low-tortuosity electrodes, a facile, cost-effective, highly controlled, and high-output continuous additive manufacturing roll-to-roll screen printing technology is proposed to render customized vertical channels within electrodes. Extremely precise vertical channels are fabricated by applying the as-developed inks, using $LiNi_{0.6}Mn_{0.2}Co_{0.2}O_2$ as the cathode material. Additionally, the relationship between the electrochemical properties and architecture of the channels, including the pattern, channel diameter, and edge distance between channels, is revealed. The optimized screen-printed electrode exhibited a seven-fold higher charge capacity (72 mAh g^{-1}) at a current rate of 6 C and superior stability compared with that of the conventional bar-coated electrode (10 mAh g^{-1}, 6 C) at a mass loading of 10 mg cm^{-2}. This roll-to-roll additive manufacturing can potentially be applied to various active materials printing to reduce electrode tortuosity and enable fast charging in battery manufacturing.

1. Introduction

The steadily expanding electric vehicle market necessitates the development of fast-charging technology for lithium-ion batteries (LIBs) to drastically increase the battery capacity at high charge densities.[1,2] In addition to investigating a new generation of materials,[3] optimizing the structure of the electrodes can help realize substantial enhancement in the capacity of LIBs at high current rates.[4] Reducing the tortuosity of electrodes is a widely established strategy for altering their structure, as this results in superior charge transfer kinetics and excellent specific capacity at high current densities compared to conventional bulk electrodes.[5,6] Creating vertical channels is a straightforward strategy to reduce the tortuosity of electrodes.

In addition to reducing the tortuosity of the electrodes, the pattern, diameter, and edge distance of the channels determine the charge transport kinetics of the electrodes. The transport kinetics not only affect the polarization and rate capabilities of electrodes but also eventually have a profound impact on the stability and safety of the electrodes.[7] Although previous reports have claimed that the increase in channel density contributes to the rate performance of low-tortuosity electrodes for fast-charging LIBs,[8–10] a comprehensive and detailed analysis of the relationship between channels and the electrochemical performance of LIBs is lacking. Understanding this relationship allows for the design of structures that optimizes the electrode and maximize the capacity of fast-charging LIBs in the future.

Roll-to-roll (R2R) screen printing is now a promising approach for the precise architectural design of electrodes, as it can effortlessly construct the pattern, diameter, and edge distance of the vertical channels within as-printed products.[11–13] Through the use of this technology, the underlying relationship between charge transport kinetics and electrode structure can be studied in details. In addition to optimizing the architecture with high precision, R2R screen printing can be integrated into existing industrial electrode manufacturing production processes.[14] Compared with the existing scalable direct channel fabrication[9,15–17] and post-treatment methods,[18] industrial R2R screen printing is simple, highly productive, controllable, and economical for mass manufacturing low-tortuosity electrodes. As a continuous additive manufacturing process, R2R screen printing increases the mass loading of the electrodes using a facile layer-by-layer printing process, which possesses higher yield and efficiency than traditional peer-to-peer 3D printing technology.[19,20] R2R screen

Y. Wang, D. Cao, T. Ji, H. Ren, H. Zhu
Department of Mechanical and Industrial Engineering
Northeastern University
Boston, MA 02115, USA
E-mail: h.zhu@neu.edu
Y. Zhang
Neutron Sciences Directorate
Oak Ridge National Laboratory
Oak Ridge, TN 37831, USA
G. Wang, Q. Wu
Department of Chemical and Paper Engineering
Western Michigan University
Kalamazoo, MI 49008, USA

The ORCID identification number(s) for the author(s) of this article can be found under https://doi.org/10.1002/smtd.202201344

DOI: 10.1002/smtd.202201344

printing, unlike reduced material manufacturing such as laser[10] and chemical etching,[18] does not generate waste and can effectively cut costs and environmental pollution.

Herein, we propose a combination of screen printing and battery electrode manufacturing to produce low-tortuosity electrodes for fast-charging LIBs industrialization. Particularly, we built and fabricated a series of tailored channels for the $LiNi_{0.6}Mn_{0.2}Co_{0.2}O_2$ cathode to comprehensively understand the effects of the pattern, channel diameter, and channel edge distance on the electrochemical properties of the electrode. At 4 and 6 C, the optimized screen-printed electrodes exhibited two- and seven-fold higher charge capacity than conventional bar-coated electrodes, respectively. Additionally, neutron computed tomography was applied to comprehend the Li distribution of the optimized screen-printed electrodes at various charge states during cycling. The results showed that the channels can promote uniform ion transfer and enhance the ion transfer kinetics on the electrodes. Additionally, R2R screen printing can be applied to the industrial production of electrodes with a well-designed structure and aid in the commercialization of fast-charging batteries.

2. Results and Discussion

Artificially created channels within the electrodes decrease the tortuosity of the electrodes. As depicted in **Figure 1**a, the channels shortened the ion transport pathway, therefore accelerating the mass transport of the electrolyteand enhancing the rate performance of thick electrodes. In contrast, the ion transport pathway within conventional bulk electrodes is much lengthened, hindering electrochemical reactions and adversely affecting the rate performance of the thick electrodes. Furthermore, Figure 1b illustrates the underlying mechanism of the enhanced fast-charging performance due to the vertically aligned channels within the electrodes, which improves ion accessibility and shorten the ion movement distance in both lateral and axial directions to enhance axial ion transfer and radial ion diffusion. Excellent accessibility and wettability between active materials and the electrolyte is a prerequisite for fast ion transportation and fast charge. For the electrodes with channels, the accessibility of the electrode and electrolyte depends on the electrode thickness, channel diameter, and channel edge distance. The wettability depends on the rheological properties of the liquid electrolyte and the surface tension between the electrode and electrolyte. In this work, the outstanding accessibility between low-tortuosity electrodes with large diameter channels and good wettability between low-viscosity liquid electrolyte and electrode ensure superior ion transportation inside electrode channels. But lithium ions are considerably smaller than the channel diameter; therefore, expanding the channel diameter over 100 μm has little benefit for the vertical ion transfer; conversely, a very large channel diameter directly decreases the energy density of the electrode. Consequently, reducing the channel diameter can effectively increase the density of the channels and facilitate vertical ion transport. Compared with the diameter of the channels, the edge distance between the channels has a stronger impact on the fast charging of the electrodes. Reducing the edge distance not only increases the channel density to benefit axial ion transport but also shortens the lateral distance of ion diffusion and further enhances the ion-transfer efficiency. In addition to benefiting ion transportation, small channels and short edge distances improve the active material density, which can further benefit the electric conductivity and mechanical stability of the whole electrode. As a result, channels with a small diameter and short edge distance simultaneously facilitate 3D ion transfer, accelerate the electric conductivity of the whole electrode, improve the electrode structural stability, and maintain a high volumetric energy density for fast-charging batteries, enabling the electrode to achieve high energy density, high rate performance, and durable cycling.

The effects of pattern and channel diameter on the electrochemical properties of electrodes were investigated at a low resolution. After screening the optimized pattern and channel diameter, the influences of the edge distances between the channels on the electrochemical performances of electrodes were understood at a high resolution with a channel diameter of 0.1 mm. Compared to low-resolution screen-printed electrodes, fabricating screen-printed electrodes with a high resolution is more challenging because the heavy flow of ink merges the channels (Figure S1a, Supporting Information). To maintain the shape of the as-printed channels and avoid patterns merging after screen printing, the viscosity of the ink was increased from honey-like (Ink 1, Figure S1b, Supporting Information) to toothpaste-like (Ink 2, Figure S1c, Supporting Information) by increasing the solid content from 60% to 68%, and the screen material was switched from polymer to stainless steel. The rheological properties of the inks are shown and discussed in Figure S1d–g (Supporting Information). All printed electrodes displayed clear and well-arranged channels when compatible inks were used. The staggered (P1) and parallel (P2) dot matrices with the same channel diameter (0.5 mm) and edge distance (2.0 mm) are shown in Figure S2 (Supporting Information). The as-printed electrodes with the same channel edge distance of 2 mm and channel diameters of 0.5, 0.7, and 1.0 mm are displayed in **Figure 2**a. The electrode material-coated regions were smooth, and the channels were clear, indicating the exceptional screen printability of the customized ink and the high printing quality of the electrodes. Subsequently, high-resolution electrodes with the same channel diameter (0.1 mm) and different edge distances (0.2, 0.3, and 0.4 mm) were printed, as shown in Figure 2b. The majority of channels were visible at high resolution. To clearly distinguish the patterns, all the electrodes were named P*a*-D*b*-E*c* according on their: pattern (P), channel diameter (D), and edge distance (E), where *a* signifies the pattern category, and *b* and *c* denote the lengths of D and E at the millimeter level, separately, as shown in Tables S1 and S2 (Supporting Information).

In order to evaluate the influences of the channel pattern and channel diameter within the printed electrodes, bar-coated and screen-printed low-resolution electrodes were printed with ink 1 and assembled in coin cells using lithium as the counter electrode. **Figure 3**a depicts the first three charge and discharge curves of the P1-D0.5-E2.0 electrode at a current rate of 0.1 C. The initial charge and discharge capacities of the P1-D0.5-E2.0 electrode were 223 and 179 mAh g^{-1}, respectively. The initial coulombic efficiency was 80.3%, which was influenced by the formation of a cathode electrolyte interface on the high specific surface of the as-printed electrode. Increased specific surface area is mostly attributable to the high-porosity structure and the vast number of channels formed during the screen printing process. Two subsequent cycles displayed similar charge and discharge capacities

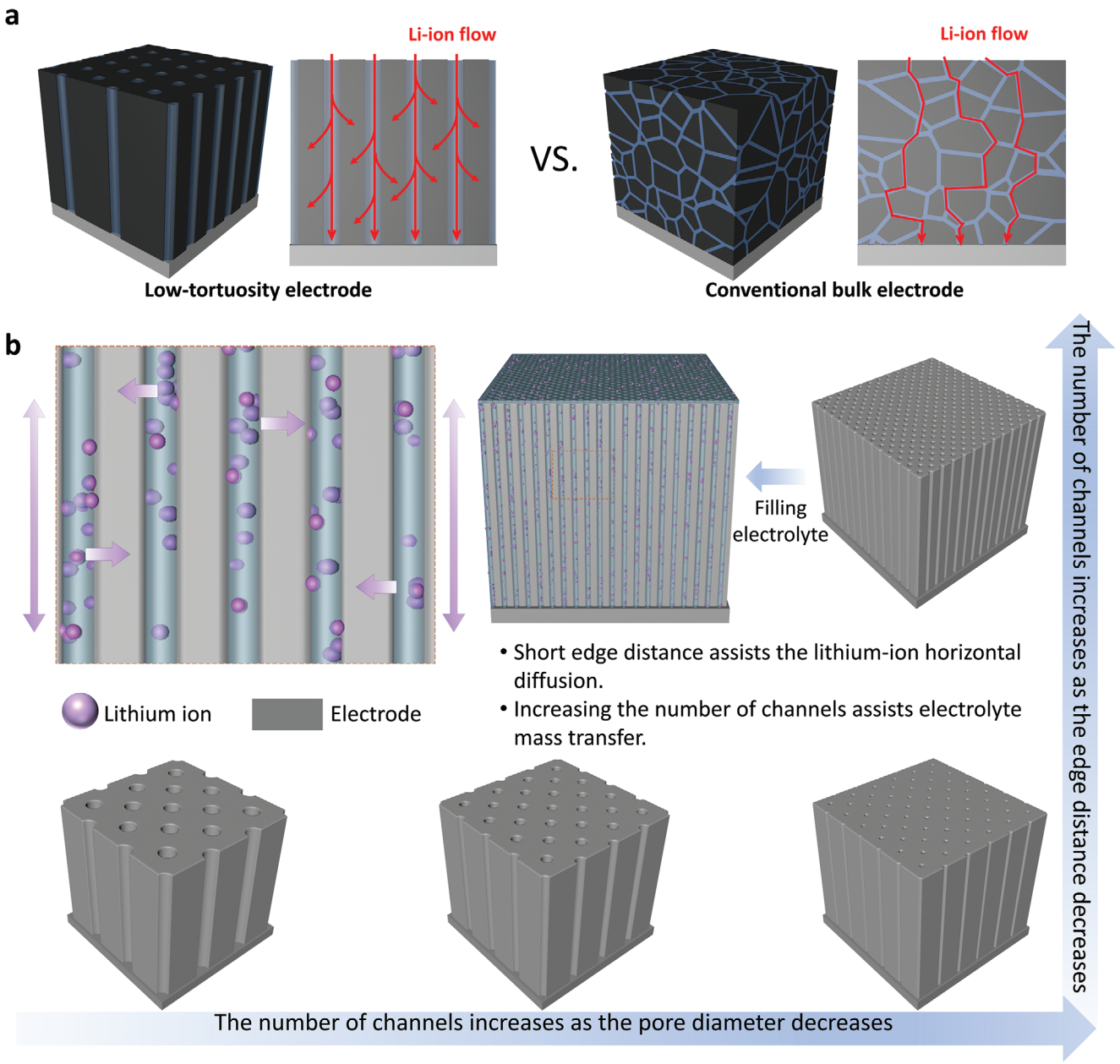

Figure 1. Advantages and conceptual design of the application of screen-printed low-tortuosity LIB electrodes. a) Schematic of lithium ions flowing through low-tortuosity and conventional bulk electrodes (High-tortuosity). b) Schematic of ion pathways in channels fabricated via screen printing.

with a coulombic efficiency of around 97.0%, indicating adequate stability. The Nyquist plots of the screen-printed electrodes with different channel patterns (Figure 3b) show semicircles following the Warburg tails. The semicircles in the high-frequency area indicate the charge transfer resistance (Figure 3c), and the Warburg tails in the low-frequency region represent the ion diffusion resistance. Evidently, the charge transfer resistances of the screen-printed electrodes were comparable but were significantly lower than that of the bar-coated electrode.

The rate performance of the electrodes was evaluated by charging at 0.1, 0.5, 1, 2, 3, 4, and 6 C and discharging at C/3 (1 C equals 180 mA g^{-1}). A comparison of the rate performances of electrodes with different channel patterns wherein the voltage hold was applied during charging from 2 to 6 C is shown in Figure 3d, but the accompanying capacity is not included in the data. The P1-D0.5-E2.0 electrode exhibited higher rate capacities than the P2-D0.5-E2.0 electrode from a current rate of 2 C. At 4 C, the charge capacity of the P1-D0.5-E2.0 electrode was 49 mAh g^{-1}, which is significantly higher than that of the P1-D0.5-E2.0 electrode (8 mAh g^{-1}). Consequently, channels arranged in a staggered matrix render high capacity for electrodes at high current rates because of the average shorter and more uniform distances between the channels. Figure 3e illustrates the charge capacity when the channel pattern was staggered and the pore

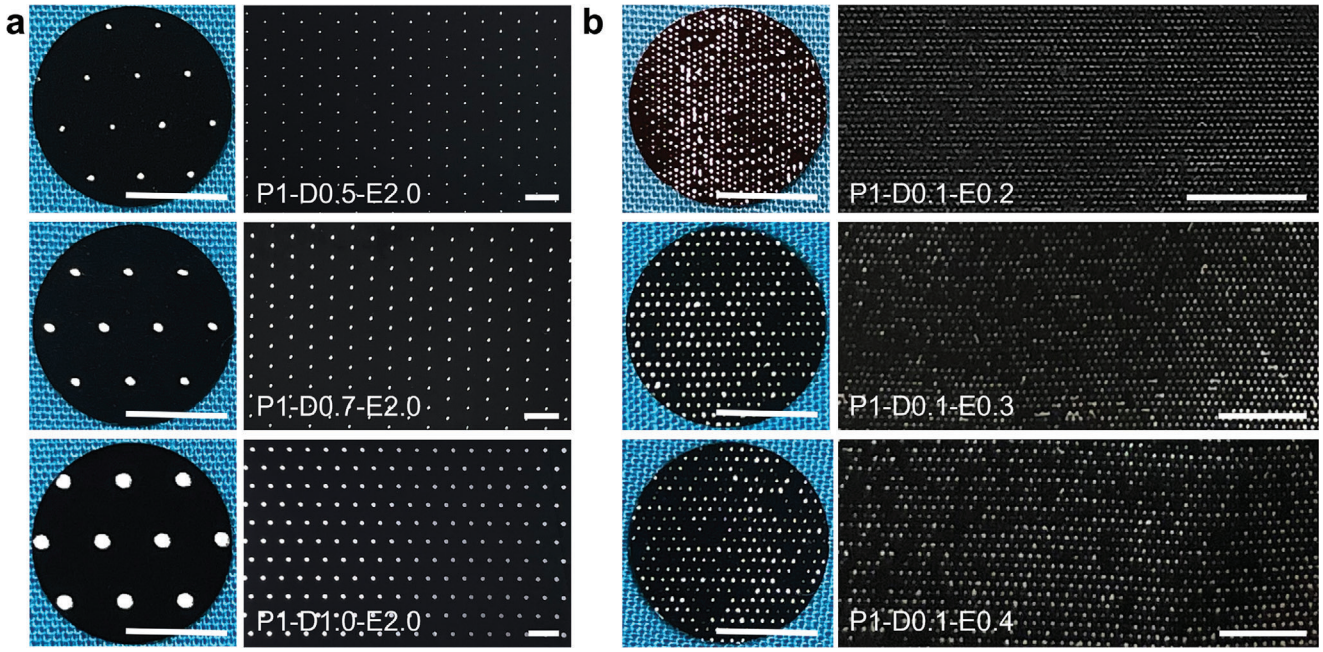

Figure 2. Printability of multilayer screen-printed electrodes with a mass loading of 10 mg cm^{-2}. a) As-printed electrodes with equal channel edge distances of 2 mm and various channel diameters of 0.5, 0.7, and 1.0 mm. b) As-printed electrodes with equal channel diameters of 0.1 mm and different channel edge distances of 0.2, 0.3, and 0.4 mm. The scale bar is 0.5 cm for all images.

diameters of the electrode were 0.5, 0.7, and 1.0 mm. All the electrodes exhibited similar charge capacities of 184, 165, 135, and 102 mAh g^{-1} at current rates of 0.1, 0.5, 1, and 2 C, respectively. The advantage of an electrode with vertical channels is apparent at high current rates of 3 and 4 C. In particular, P1-D0.5-E2.0 had the highest specific charge capacity (49 mAh g^{-1}) among all the electrodes at a current rate of 4 C. The long-term stability of these electrodes was evaluated with a charge rate of 1 C and a discharge rate of C/3, as shown in Figure 3f. Cells were activated by charging at 0.1 C and discharging at C/3 for five cycles. Among all the screen-printed electrodes, the P1-D0.5-E2.0 electrode displayed superior stability after 70 cycles, which is because more electrode materials covered the current collector and the adhesion between the electrode and the current collector was stronger. Additionally, the coulombic efficiency of the P1-D0.5-E2.0 electrode was exceeded 98.5% for the 100th cycle. With the same ink, the bar-coated electrode displayed an unexpected vibration at 32 cycles and a rapid decline at 42 cycles, indicating poor stability. In contrast to the screen-printed electrodes, no vertical pressure was applied during manufacturing bar-coated electrodes, which led to a weak connection between the electrode and the current collector and destabilized its cycling stability. The mechanical stability of the electrode on the current collector was evaluated using the tape peeling method (Figure S3, Supporting Information), which shows an intensive particle release from the bar-coated electrode. Comparatively, the P1-D0.5-E2.0 electrode retains the greatest number of solid particles.

Following the previous filtering of the matrix and channel diameter of screen-printed electrodes, a staggered dot matrix (P1) with a channel diameter of 0.1 mm was selected as a channel pattern and channel diameter to optimize the rate performance of the screen-printed electrodes with channel edge distances of 0.2, 0.3, and 0.4 mm. A diameter of 0.1 mm is the smallest dot diameter currently available in industrial microscreen manufacturing for screen printing. The cyclic voltammetry (CV) curves of the screen-printed and bar-coated electrodes (**Figure 4**a) show apparent oxidation (≈3.9 V) and reduction (≈3.6 V) peaks without significant additional peaks, suggesting that there was no side reaction during screen printing. Moreover, the screen-printed electrodes displayed smaller potential gaps than the bar-coated electrodes, indicating superior reaction kinetics and lower polarization. Figure 4b shows the initial three galvanostatic charge and discharge curves of the P1-D0.1-E0.2 electrode at a current rate of 0.1 C. The initial charge capacity of the P1-D0.1-E0.2 electrode was 209 mAh g^{-1} with the initial coulombic efficiency of 84.7%. The following two cycles exhibited a similar specific charge capacity of 182 mAh g^{-1}, suggesting reasonable stability of the P1-D0.1-E0.2 electrode. The Nyquist plots of the screen-printed high-resolution electrodes are shown in Figure S4 (Supporting Information) and Figure 4c. The intercept distance and the diameter of the semicircle indicate the bulk and charge transfer resistances of the electrodes, respectively. The bulk and charge transfer resistances of the screen-printed electrodes were similar, and both of them were smaller than those of the bar-coated electrodes. The charge transfer resistance reduction of screen-printed electrodes is consistent with prior findings at low resolution (Figure 3c) since the vertical channels created by screen printing can improve the charge transfer kinetics and reduce the charge transfer resistance of the electrodes.

The rate performances of the screen-printed and bar-coated electrodes are compared in Figure 4d at charging current rates of 0.1, 0.5, 1, 2, 3, 4, and 6 C and discharging at C/3. A voltage hold was applied during charging from 2 to 6 C, but the associated capacitance is not included in the data. The electrodes with

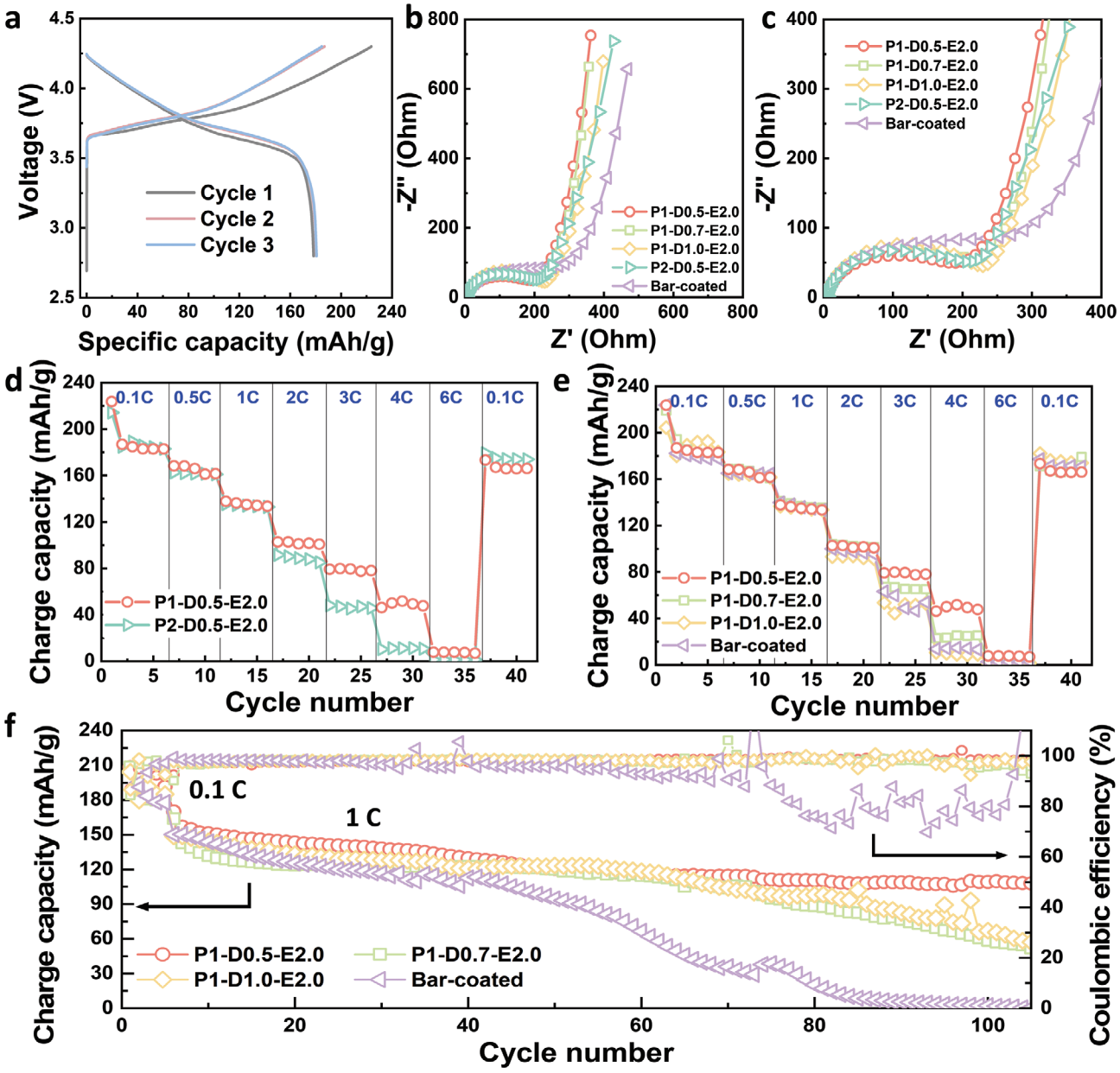

Figure 3. Electrochemical performances of screen-printed electrodes in low resolution. All electrodes were prepared with Ink 1. a) Galvanostatic charge-discharge curves of the initial three cycles of the P1-D0.5-E2.0 electrode. b,c) Nyquist plots of electrodes. d) Rate performances of as-printed electrodes with different channel patterns of P1 and P2 and e) bar-coated and screen-printed electrodes possessing the same channel pattern, P1, with an edge distance of 2.0 mm and various channel diameters of 0.5, 0.7, and 1.0 mm. f) Long-term cycling performance of screen-printed electrodes with same channel edge distance and different channel diameters.

channels exhibited superior charge capacities than the bar-coated electrode in the range of 0.5–6 C. As the current density flow increased, the disparity between the charge capacities of the electrodes enlarged. Although all the screen-printed electrodes exhibited similar specific charge capacities of 182, 169, 151, 130, 118, and 96 mAh g^{-1} at current rates of 0.1, 0.5, 1, 2, 3, and 4 C, respectively, the effect of the edge distance on the electrodes was noticeable at a high current rate of 6 C. When the current rate was increased to 6 C, the electrodes with channels exhibited charge capacities of 72, 57, and 44 mAh g^{-1} as the edge distances rose to 0.2, 0.3, and 0.4 mm, respectively. Notably, P1-D0.1-E0.2 exhibited the highest specific charge capacity among screen-printed electrodes, which was sevenfold higher than that of the bar-coated electrode (10 mAh g^{-1}) at 6 C.

The charge curves of P1-D0.1-E0.2 and the bar-coated electrodes at various charging current rates are shown in Figure S5a (Supporting Information), and the potential gaps of the electrodes at the 20% state-of-charge (36 mAh g^{-1}) and the voltage cutoff (2.8 V) are shown in Figure S5b (Supporting Information). The bar-coated electrode showed a larger potential gap, and the

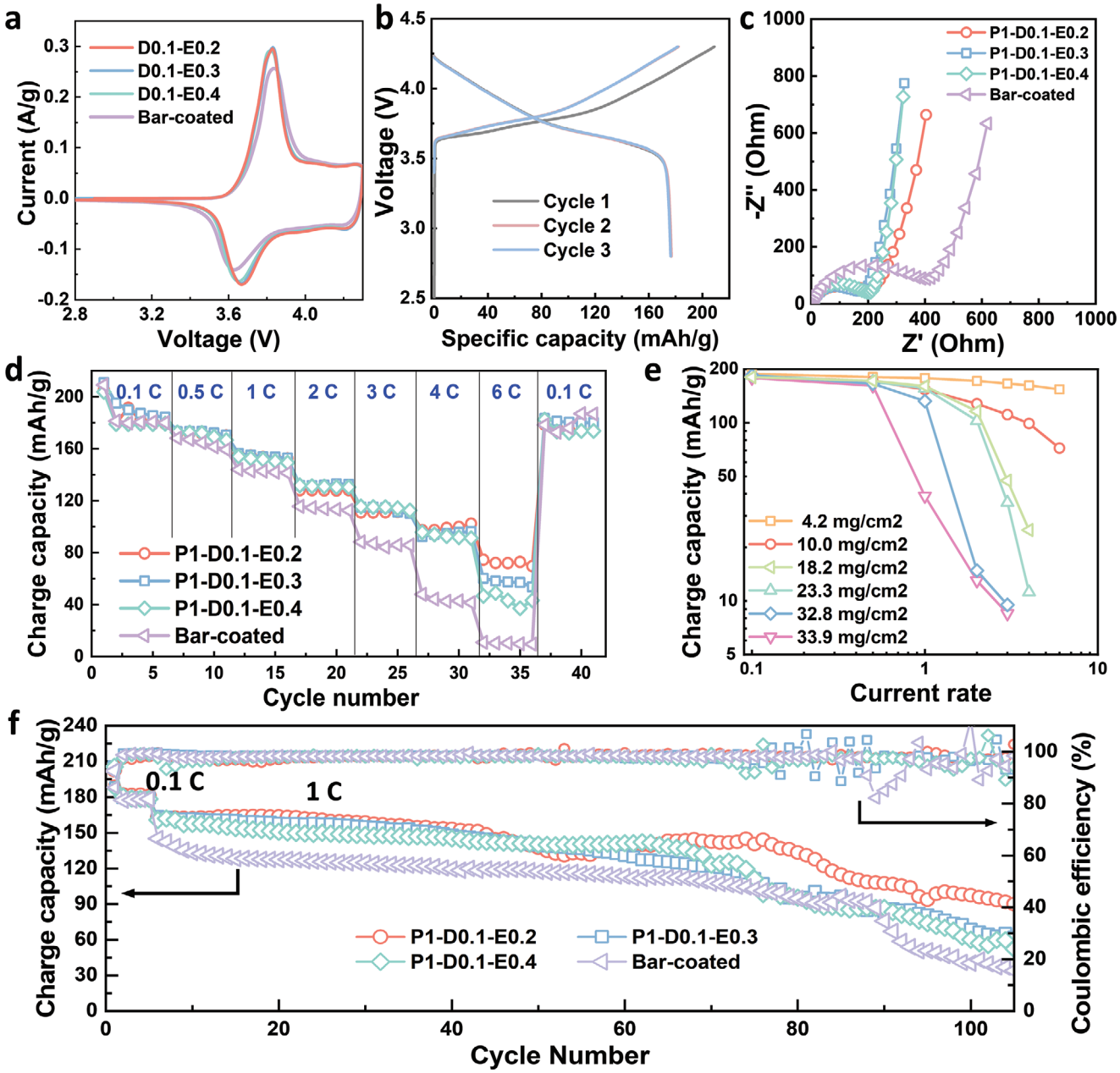

Figure 4. Electrochemical performances of screen-printed electrodes with P1 patterns in high resolution. All electrodes were prepared with Ink 2. a) Galvanostatic charge-discharge curves of the initial three cycles of the P1-D0.1-E0.2 electrode. b,c) Nyquist plots and d) rate performances of bar-coated and screen-printed high-resolution electrodes. e) Rate performances of P1-D0.1-E0.2 electrodes with different mass loadings. f) Long-term cycling performance of bar-coated and screen-printed electrodes.

difference increased with increasing current density, indicating superior electrochemical kinetics of the P1-D0.1-E0.2 electrode than that of the bar-coated electrode, particularly at high current rates. The rate performance of P1-D0.1-E0.2 electrodes with various mass loadings are compared in Figure 4e, revealing that the higher electrode mass loading is accompanied with a more pronounced charge capacity decay with the current density elevating. With a rise in the mass loading, the thickness of the electrodes increased, resulting in an increase in the charge transfer distance and a decrease in the charge transfer kinetics.

The long-term cycling performances of the electrodes at a charge rate of 1 C and a discharge rate of C/3 are depicted in Figure 4f, and they were initially activated at 0.1 C for five cycles. Although all electrodes showed a notable capacity decline at approximately 85 cycles, P1-D0.1-E0.2 exhibited better stability. The superior stability of the screen-printed electrodes can be attributed to the optimized channels that mitigate the electrodes architectural damage caused by lithium-ion insertion and stripping. The shorter the channel edge distance, the higher the channel density, and the less irreversible collapse within the electrode

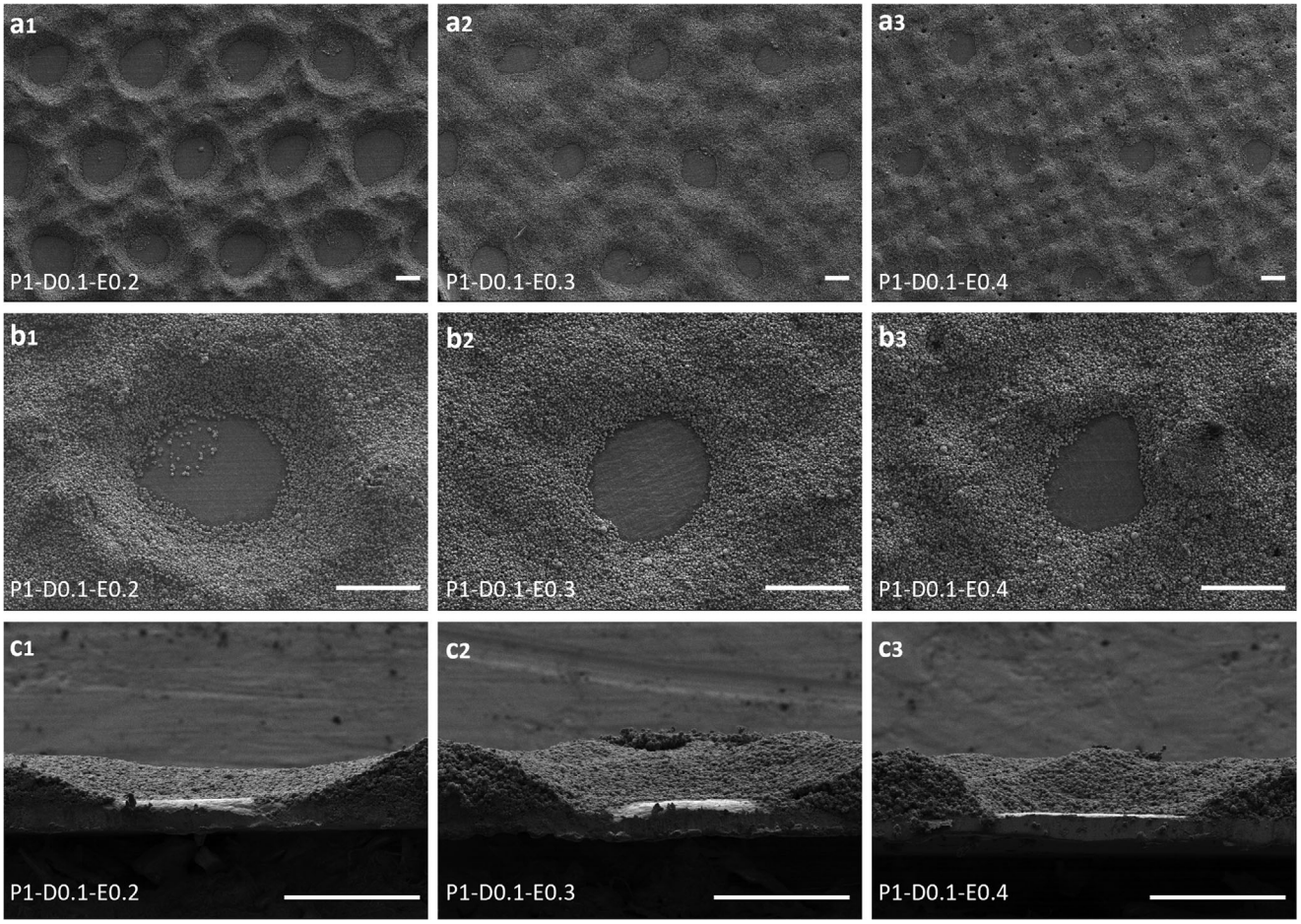

Figure 5. SEM images of one-layer printed electrodes with staggered channel matrix. Top view of a1,b1) D0.1-E0.2, a2,b2) D0.1-E0.3, and a3,b3) D0.1-E0.4 electrodes. Cross section of c1) D0.1-E0.2, c2) D0.1-E0.3, and c3) D0.1-E0.4 electrodes. The scale bar is 100 μm for all images.

is mitigated. Therefore, the poor structural stability of the bar-coated electrode results from the limited room available for alleviating the internal pressure during lithium-ion migration.

The morphology of the electrodes with high-resolution channels was further characterized using scanning electron microscopy (SEM). **Figures 5**a1–a3 display the top view of the screen-printed channels. All the channels were clear, had a reasonably round form, and was composed of a regular pattern, which is consistent with the pattern design. Regular bumpy craters were observed between the channels of the P1-D0.1-E0.3 (Figure 5a2) and P1-D0.1-E0.4 (Figure 5a3) electrodes. The magnified image (Figure S6, Supporting Information) of these bumpy craters shows neatly arranged similar deep square depressions with a length of ≈80 μm. These craters are the imprints created by the low fluidity of the ink as it passes through the screen fibers. Figures 5b1–b3 display the channels of the corresponding electrodes at high magnification, and Figures 5c1–c3 show their cross-sectional images. Bare aluminum foil areas were uncovered at the bottom of the printed electrodes. Since the inevitable shrinkage of the electrode material-covered area during the drying process, the diameter of the channels was slightly larger than 100 μm. The relationship between the electrode-covered area shrinkage and channel enlargement throughout the drying process of the low-resolution screen-printed electrodes is shown in Figures S7 and S8 (Supporting Information), respectively. Although patterns and diameter of channels affect the change ratio of screen-printed channels, the channel did expand by ≈110% for 30 min of drying. Moreover, the channels exhibited a distinct bowl-like structure, resulting from the unavoidable flow of the ink.

The exceptional rate performance of the screen-printed electrodes is attributed to the vertical channel, which effectively optimizes the lithium distribution during cycling. To understand the mechanism of channels in improving the charge capacity of screen-printed electrodes more intuitively, lithium distribution inside P1-D0.1-E0.2 electrodes was characterized using neutron computed tomography. **Figure 6**a plots the voltage presents voltage vs. state of charge (SOC) of electrodes and the actual capacity of the electrode material is used to calculate the SOC of samples. Figure 6b shows the lithium distribution within channels with longitudinally aligned electrodes at various SOC. Red indicates the lithium-rich regions whereas greenish-blue represents regions with low lithium concentrations. Figure 6c shows the lithium distribution in the aforementioned electrodes along their width (left to right) and length (top to bottom). With cathode delithiation, the red weakens homogeneously. The electrode

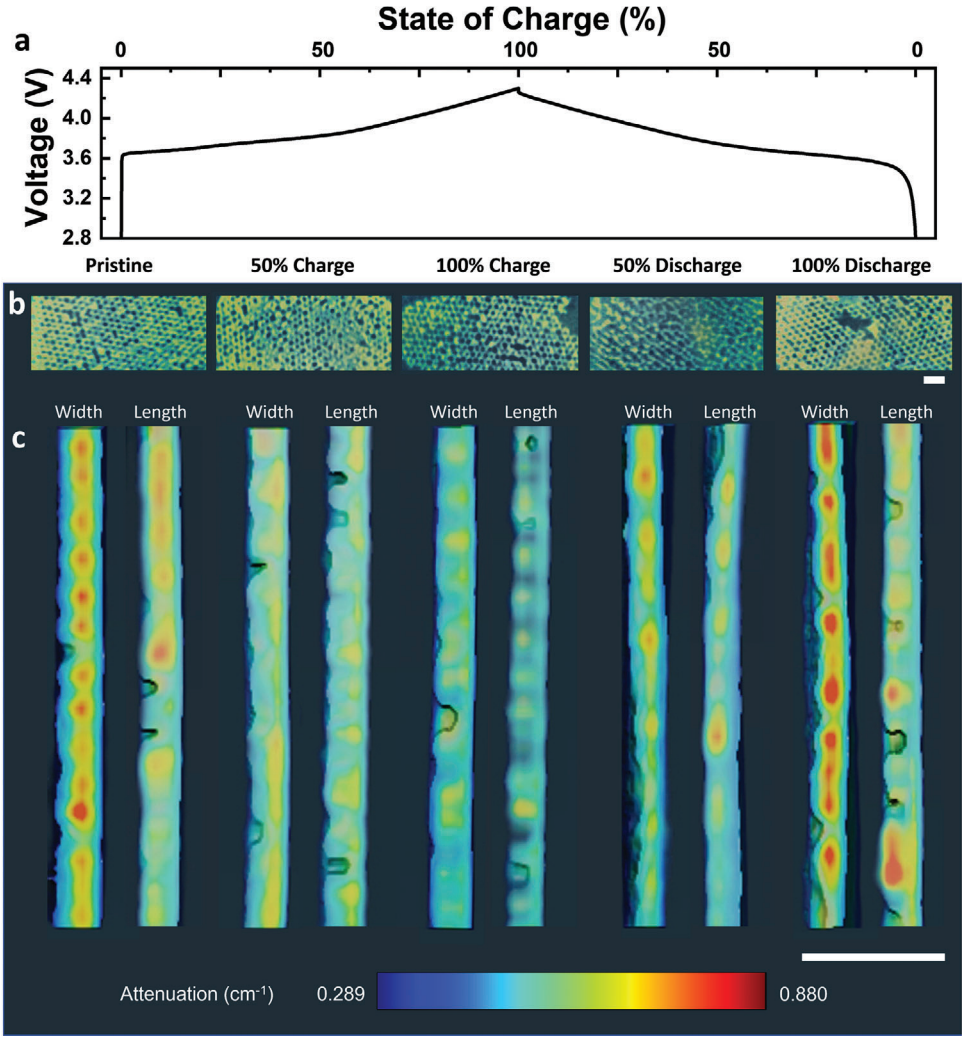

Figure 6. Lithium distribution in screen-printed channel-integrated electrodes at various charging and discharging stages. a) Voltage vs. state of charge curve, b) top view and c) cross-sectional view of pristine, 50% charge, 100% charge, 50% discharge, and 100% discharge electrodes. The red region in the figures represents enriched lithium, while the blue region corresponds to diminishing Li. The diameter of the channels is 0.1 mm, and the edge distance of the channels is 0.2 mm. Scale bars are 1 mm.

charged to 100% exhibited a large amount of blue region with a few yellow areas, indicating lithium extraction until charging was complete. With cathode lithiation, lithium diffused into the cathode, and a very strong red signal can be observed at the fully discharged electrode. Additionally, along the channel-built direction, the yellow and red areas show a regular rod-like distribution on the electrodes, suggesting that more lithium migrated along the channels. Meanwhile, the evenly colored signal of lithium (red and yellow) can be observed throughout the entire electrode, indicating that channels enabled the lithium distribution to be uniform from the separator side to the current collector side. Figure S9 (Supporting Information) shows the assembly of the cells in detail. Consequently, the channel aids in preventing ions from singularly accumulating on the electrode surface and in enhancing the reaction kinetics on the current collector side of the electrodes during cycling. The enhanced mass transfer kinetics improve the capacitance of the electrodes, particularly at high current rates.

Although printed channels can improve electrode rate performance and structural stability, further printing specifics must be explored to realize the highest capability of the electrodes for industrialization. For instance, although researchers anticipate obtaining high-accuracy and high-resolution printed products, the challenges in screen printing technology markedly increase as the resolution increases from the millimeter to the micron level. Specifically, the diameter and edge distance of the customized channels directly affect the difficulty of printing in this work, a plot of which as a function of these variables is shown in **Figure 7**a; the redder the color, the higher the printing difficulty. The printing difficulty increases as the channel diameter and edge distance reduce, which can be attributed to the three factors described next. Firstly, an ultrahigh resolution of several micros is temporarily unattainable. Limited by the current technology, the wire diameter of commercially available metal mesh is limited to 18 μm with a mesh opening of 46 μm;[21] the channel diameter is limited to ≈100 μm to ensure that a circular pattern

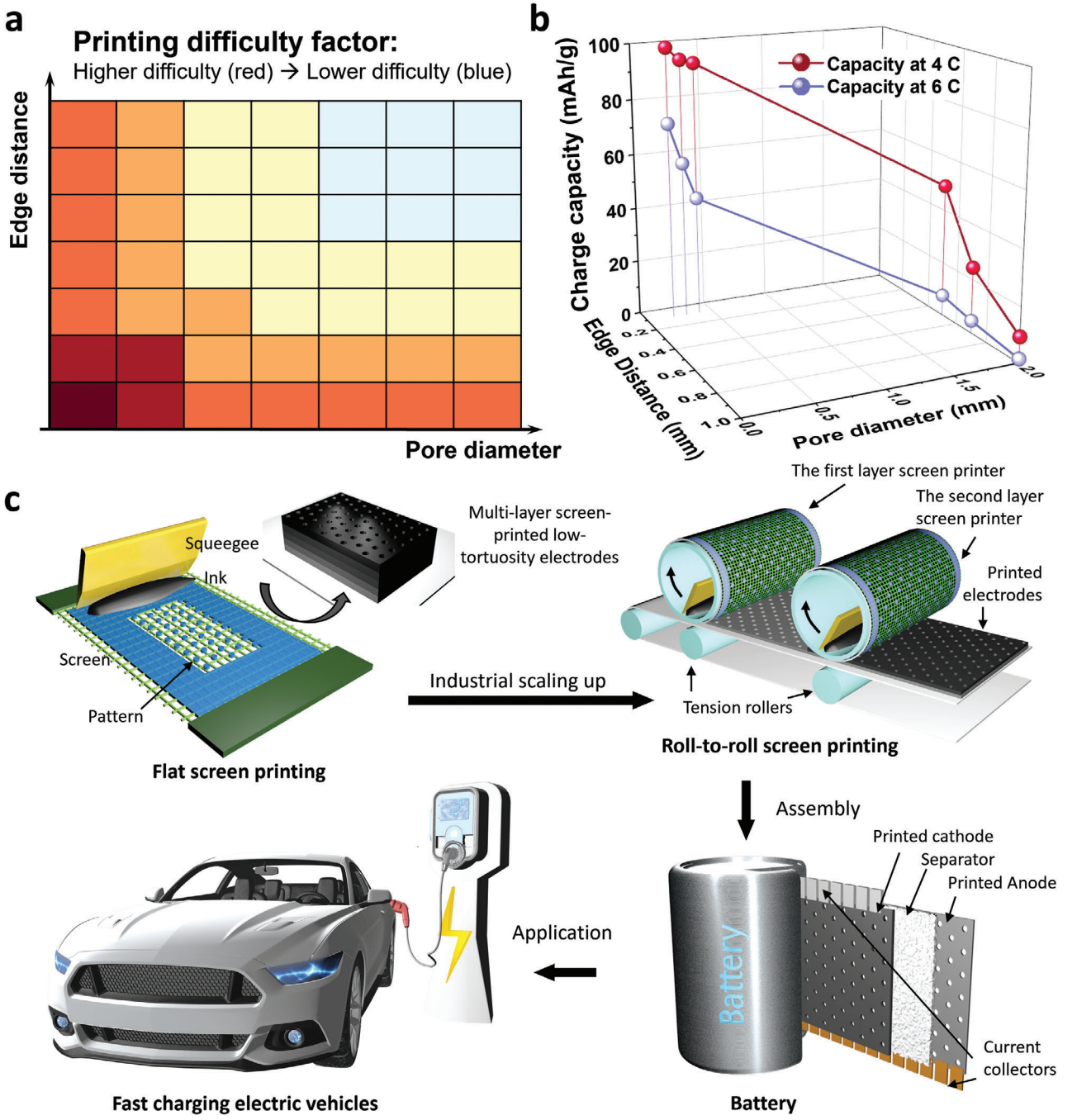

Figure 7. Summary of effects of vertical channel diameter and edge distance on a) screen printing difficulty and b) fast-charging capacity. c) Low-tortuosity electrode fabrication processes through screen printing on laboratory- and industry-scale, and battery assembly and application of this technology in electric vehicles.

emulsion is carried on two wires of the screen to maintain a stable shape before and after screen printing. Second, the ink should have low fluidity to avoid the merging of printed patterns and provide a high resolution. However, the lower fluidity indicates a tighter internal structure, and such a structure is resistant to squeezing through the tiny gaps of fine screens. Thirdly, the higher the resolution, the less accurate the design patterns will be because the fibers drag ink units and obstruct ink transfer to the substrate during the printing process. The aforementioned results suggest that a smaller channel diameter and shorter edge distance between channels lead to better rate performance of screen-printed LIB electrodes at high current densities (Figure 7b). Therefore, higher-resolution microscreen production and more investigations of the design of the channels in the electrodes are necessary to achieve a satisfactory fast-charging capacity.

In addition to presenting a straightforward approach for investigating the channels within the electrodes and effectively improving the electrochemical performance at high current rates, it is believed that screen printing can be integrated into existing production processes and satisfy industrial manufacturing requirements. As shown in Figure 7c, we fabricated screen-printable electrode inks, created bespoke channels inside the electrodes using screen printing, and increased the thickness and mass loading of the electrodes by multiple printing. Figure S10 (Supporting Information) exhibits the screen-printed electrodes in a large area with an advanced flat-screen printer, demonstrating its potential to be industrialized. Similarly, the R2R screen printing can be applied to manufacture low-tortuosity electrodes, wherein the multi-roller can be assembled to enhance and control the mass loading of printed electrodes for commercialization. The details of an R2R screen printer are shown in Figure S11 (Supporting Information), in which a squeegee and an ink tank are built into the roller screen. It is evident that the proposed continuous R2R screen printing battery manufacturing technology satisfies industrialization and commercialization requirements because it is facile to control and scalable with no material wastage or impurity introduction.

3. Conclusion

In this study, we demonstrated an R2R screen printing technology to create tailored channels and impart a low-tortuosity architecture within electrodes, which can be used industrially in fast-charging LIBs. Applying a custom ink, we successfully rendered screen-printed LIBs electrodes with customized channels of high resolution. Additional research indicates that the pattern, diameter, and edge distance between the channels affect the rate performance and stability of the electrodes. Specifically, channels with staggered patterns exhibited a higher rate performance than channels with parallel patterns. Concurrently, the fast-charging capacity of screen-printed electrodes increases simultaneously with a reduction in the channel diameter and a shortening of the channel edge distance. Superior to the conventional bar-coated electrode, the screen-printed electrode with staggered channels with 0.1 mm diameter and 0.2 mm edge distance exhibited a sevenfold higher specific charge capacity at 6 C. During charging and discharging, lithium was evenly distributed along all channels, and ions were effortlessly transferred to the side that connects to the current collector, thereby enhancing the rate performance of the screen-printed electrodes. Furthermore, the short edge distance between channels expedited the ion diffusion in the radial direction. Despite further investigation is required to reduce the difficulty of screen printing at a high resolution and optimize the design of channels, as a facile, high-output, and cost-effective continuous additive manufacturing technique, R2R screen printing offers new opportunities for the industrial manufacture of fast-charging batteries and promises to accelerate the development of electric vehicles.

4. Experimental Section

Materials: Polycrystalline NMC 622 was obtained from Nanoramic Laboratories. Super P and aluminum foil current collectors were procured from MTI Corporation. Homopolymer PVDF (Kureha 7200 with an average molecular weight of 6.3×10^5 g mol^{-1}) was procured from Kureha Company. NMP was procured from Fisher Science Education. Before preparation of the ink, NMC 622 and Super P powders were dried for at least 12 h at 100 °C, and the homopolymer PVDF was dissolved into NMP to achieve the concentration of 10 wt.%. All materials were used without any additional treatment.

Ink Preparation: All inks were prepared as NMC 622, Super P, and PVDF with weight ratios of 92:5:3 in the formulation and 3 g for a total weight of solid materials per batch. Herein, Ink 1 with 60% solid content, and Ink 2 with 68% solid content were prepared to satisfy the various printing situations. All components were thoroughly mixed with a dual asymmetric centrifugal mechanism (DAC 330-100 Pro Speedmixer from Flak-Tek).

Screen Printing: The pattern for electrode printing was designed using Adobe Illustrator software (Adobe Inc.). The low-resolution patterns with 0.5, 0.7, and 1.0 mm channel diameters and 2.0 mm edge distance were loaded on a 300 mesh polymer screen, and the thickness of the total screen and emulsion was ≈60 µm for electrode printing. The high-resolution patterns with 0.1 mm channel diameter and 0.2, 0.3, and 0.4 mm edge distances were loaded on a 325 mesh stainless steel screen (Microscreen Inc.). The emulsion thickness was 15 µm, and the screen thickness was 28 µm. The aluminum foil was used as both the current collector and substrate to evaluate the electrochemical properties of the screen-printed electrodes.

Characterization Methods: The morphology of the samples was observed by SEM (Hitachi S4800) at 3 kV. Optical microscopy characterization of the printed channels during the drying process was done with an Olympus VANOX-T optical microscope. The rheological properties were measured by a discovery hybrid rheometer (Discovery HR-30) from TA-Instruments with a flat Peltier plate. The tape peeling method was performed using 3 M 6122 MP Scotch Magic Tape under a standard of ASTM D3330, method A.

Neutron Characterization: Neutron imaging was performed at the cold neutron imaging beamline CG-1D at the High Flux Isotope Reactor (HFIR) at Oak Ridge National Laboratory, USA. The washed electrodes with various SOC were stuck on a thin aluminum plate for neutron computed tomography (CT) scan. During the CT scan, the plate was mounted on a rotation stage to collect a 30 s exposure image at every 0.37 through a 0-360 rotation. The collected images were then loaded into MuhRec[22] for 3D volume reconstruction. The reconstructed volume was visualized and analyzed using Amira-Avizo 3D software.[23]

Electrochemistry Characterization: All electrochemical measurements were tested at room temperature, and all electrodes were assembled in a 2025 coin cell set. The 80 µL Gen 2 (1.2 M $LiPF_6$ dissolved in EC: EMC = 3: 7 by weight), Celgard 2400, and lithium metal were separately used as an electrolyte, separator, and anode in the coin cells. The active materials mass loading of screen-printed and bar-coated electrodes was ≈10.0 mg cm^{-2}. The electrochemical station (Biologic SP150) was applied to evaluate the EIS performance of coin cells in the frequency range of 1 MHz to 100 mHz at room temperature, and Biologic MPG2 was used to evaluate the cyclic voltammetry (CV) curves in the range of 2.8–4.3 V and the scan rate of 0.1 mV s^{-1}. LANDT 8-channel tester (Wuhan LAND Electronic Co., Ltd.) was used to perform galvanostatic tests. For all tests, the rate performances were evaluated by charging at different C-rate, specifically 0.1 C for six cycles, then 0.5, 1, 2, 4, 6, and 0.1 C for five cycles, respectively, following discharging at the constant current rate of C/3. All the electrochemical tests were run at room temperature.

Supporting Information

Supporting Information is available from the Wiley Online Library or from the author.

Acknowledgements

H. Z. acknowledges the support by the U.S. Department of Energy's Office on Energy Efficiency and Renewable Energy (EERE) under the Advanced

Manufacturing Office, award number DE-EE0009111. The authors appreciate Nanoramic Laboratories (Wakefield, MA 01880, USA) for providing polycrystalline NMC 622 for this study. The authors thank Northeastern University Center for Renewable Energy Technology (NUCRET) for the use of SEM. This research used resources at the High Flux Isotope Reactor, a DOE Office of Science User Facility operated by the Oak Ridge National Laboratory. This manuscript has been authored by UT-Battelle, LLC, under contract DE-AC05-00OR22725 with the US Department of Energy (DOE). This article has been contributed to by US Government contractors and their work is in the public domain in the USA.

Conflict of Interest

The authors declare no conflict of interest.

Data Availability Statement

Research data are not shared.

Keywords

continuous additive manufacturing, fast-charging, low-tortuosity, screen printing, vertical channel design

Received: October 17, 2022
Revised: December 27, 2022
Published online:

[1] A. Tomaszewska, Z. Chu, X. Feng, S. O'Kane, X. Liu, J. Chen, C. Ji, E. Endler, R. Li, L. Liu, *eTransportation* **2019**, *1*, 100011.
[2] S. Li, K. Wang, G. Zhang, S. Li, Y. Xu, X. Zhang, X. Zhang, S. Zheng, X. Sun, Y. Ma, *Adv. Funct. Mater.* **2022**, *32*, 2200796.
[3] M. Weiss, R. Ruess, J. Kasnatscheew, Y. Levartovsky, N. R. Levy, P. Minnmann, L. Stolz, T. Waldmann, M. Wohlfahrt-Mehrens, D. Aurbach, *Adv. Energy Mater.* **2021**, *11*, 2101126.
[4] Y. Kuang, C. Chen, D. Kirsch, L. Hu, *Adv. Energy Mater.* **2019**, *9*, 1901457.
[5] L. Shen, Z. Chen, *Chem. Eng. Sci.* **2007**, *62*, 3748.
[6] T.-T. Nguyen, A. Demortière, B. Fleutot, B. Delobel, C. Delacourt, S. J. Cooper, *npj Comput. Mater.* **2020**, *6*, 123.
[7] X. Zhang, Z. Ju, Y. Zhu, K. J. Takeuchi, E. S. Takeuchi, A. C. Marschilok, G. Yu, *Adv. Energy Mater.* **2021**, *11*, 2000808.
[8] C. J. Bae, C. K. Erdonmez, J. W. Halloran, Y. M. Chiang, *Adv. Mater.* **2013**, *25*, 1254.
[9] J. Sander, R. M. Erb, L. Li, A. Gurijala, Y.-M. Chiang, *Nat. Energy* **2016**, *1*, 16099.
[10] J. Park, C. Jeon, W. Kim, S.-J. Bong, S. Jeong, H.-J. Kim, *J. Power Sources* **2021**, *482*, 228948.
[11] H. Emani, X. Zhang, G. Wang, D. Maddipatla, T. Saeed, Q. Wu, W. Lu, M. Z. Atashbar, in *IEEE Int. Conf. on Flexible and Printable Sensors and Systems (FLEPS)*, IEEE, New York **2021**, pp. 1–4.
[12] S. Ahmadi, Y. Wang, D. Maddipatla, D. Cao, H. Zhu, Q. Wu, M. Z. Atashbar, in *IEEE Int. Conf. on Flexible and Printable Sensors and Systems (FLEPS)*, IEEE, New York **2022**, p. 1.
[13] Y. Wang, J. He, D. Cao, E. Cakmak, X. Zhao, Q. Wu, Y. Zhao, H. Ren, X. Sun, Y. Li, *Energy Storage Mater.* **2023**, *55*, 42.
[14] Y. Wang, D. Cao, X. Sun, H. Ren, T. Ji, X. Jin, J. Morse, B. Stewart, H. Zhu, *Adv. Mater. Technol.* **2022**, *7*, 2200303.
[15] R. Xiong, Y. Zhang, Y. Wang, L. Song, M. Li, H. Yang, Z. Huang, D. Li, H. Zhou, *Small Methods* **2021**, *5*, 2100280.
[16] J. Billaud, F. Bouville, T. Magrini, C. Villevieille, A. R. Studart, *Nat. Energy* **2016**, *1*, 16097.
[17] D. P. Singh, F. M. Mulder, A. M. Abdelkader, M. Wagemaker, *Adv. Energy Mater.* **2013**, *3*, 572.
[18] W. McSweeney, H. Geaney, C. O'Dwyer, *Nano Res.* **2015**, *8*, 1395.
[19] C. Costa, R. Gonçalves, S. Lanceros-Méndez, *Energy Storage Mater.* **2020**, *28*, 216.
[20] H. Tetik, Y. Wang, X. Sun, D. Cao, N. Shah, H. Zhu, F. Qian, D. Lin, *Adv. Funct. Mater.* **2021**, *31*, 2103410.
[21] https://www.microscreenllc.com/frames-and-mesh. (accessed January 2023).
[22] A. P. Kaestner, *Nucl. Instrum. Methods in Phys. Res. Section A: Accelerators, Spectrometers, Detectors Associated Equipment* **2011**, *651*, 156.
[23] D. Stalling, M. Westerhoff, H.-C. Hege, *Visualization Handbook* **2005**, 749.

